Development/Plasticity/Repair

An Atoh1-S193A Phospho-Mutant Allele Causes Hearing Deficits and Motor Impairment

Wei Rose Xie,[1,2,3] Hsin-I Jen,[4] Michelle L. Seymour,[5,6] Szu-Ying Yeh,[1,4] Fred A. Pereira,[5,6,7] Andrew K. Groves,[3,4,8] Tiemo J. Klisch,[1,3] and Huda Y. Zoghbi[1,2,3,4,9]

[1]Jan and Dan Duncan Neurological Research Institute, Texas Children's Hospital, Houston, Texas 77030, [2]Program in Integrative Molecular and Biomedical Sciences, [3]Department of Molecular and Human Genetics, [4]Program in Developmental Biology, [5]Huffington Center on Aging, [6]Department of Molecular and Cellular Biology, [7]Bobby R Alford Department of Otolaryngology, Head and Neck Surgery, and [8]Department of Neuroscience, and [9]Howard Hughes Medical Institute, Baylor College of Medicine, Houston, Texas 77030

Atonal homolog 1 (Atoh1) is a basic helix-loop-helix (bHLH) transcription factor that is essential for the genesis, survival, and maturation of a variety of neuronal and non-neuronal cell populations, including those involved in proprioception, interoception, balance, respiration, and hearing. Such diverse functions require fine regulation at the transcriptional and protein levels. Here, we show that serine 193 (S193) is phosphorylated in Atoh1's bHLH domain *in vivo*. Knock-in mice of both sexes bearing a GFP-tagged phospho-dead S193A allele on a null background (*Atoh1*$^{S193A/lacZ}$) exhibit mild cerebellar foliation defects, motor impairments, partial pontine nucleus migration defects, cochlear hair cell degeneration, and profound hearing loss. We also found that *Atoh1* heterozygous mice of both sexes (*Atoh1*$^{lacZ/+}$) have adult-onset deafness. These data indicate that different cell types have different degrees of vulnerability to loss of Atoh1 function and that hypomorphic *Atoh1* alleles should be considered in human hearing loss.

Key words: Atoh1; hearing loss; inner ear; Math1; phosphorylation; ponti nucleus

Significance Statement

The discovery that Atonal homolog 1 (Atoh1) governs the development of the sensory hair cells in the inner ear led to therapeutic efforts to restore these cells in cases of human deafness. Because prior studies of *Atoh1*-heterozygous mice did not examine or report on hearing loss in mature animals, it has not been clinical practice to sequence *ATOH1* in people with deafness. Here, in seeking to understand how phosphorylation of Atoh1 modulates its effects *in vivo*, we discovered that inner ear hair cells are much more vulnerable to loss of Atoh1 function than other Atoh1-positive cell types and that heterozygous mice actually develop hearing loss late in life. This opens up the possibility that missense mutations in *ATOH1* could increase human vulnerability to loss of hair cells because of aging or trauma.

Introduction

Atonal homolog 1 (Atoh1) is a proneural basic helix-loop-helix (bHLH) transcription factor that plays a critical role in a variety of developmental contexts. In the nervous system, Atoh1 is required for the generation of many brainstem neurons and multiple components of the proprioceptive and interoceptive systems; it also regulates the proliferation and differentiation of cerebellar granule neurons (CGNs) (Ben-Arie et al., 1997; Bermingham et al., 2001; Wang et al., 2005). Beyond the nervous system, Atoh1 regulates the development of Merkel cells, secretory cells of the intestine, and the hair cells of the inner ear (Bermingham et al., 1999; Yang et al., 2001; Maricich et al., 2009). With such diverse roles, precise regulation of Atoh1 at both the transcriptional and protein levels is essential.

Although the transcriptional regulation of *Atoh1* has been well studied, with many factors identified that bind to the enhancer

Received Jan. 31, 2017; revised June 20, 2017; accepted June 29, 2017.

Author contributions: A.K.G., T.J.K., and H.Y.Z. designed research, reviewed data, and edited the manuscript; W.R.X., H.-I.J., M.L.S., S.-Y.Y., and F.A.P. performed research; W.R.X. and S.-Y.Y. analyzed data; W.R.X. wrote the paper.

This work was supported in part by the Neuropathology Core of the Jan and Dan Duncan Neurological Research Institute with expert assistance from Roy Sillitoe, Ph.D., and Tao Lin and also by the RNA In Situ and Microscopy and the Neurobehavioral Cores supported by a National Institutes of Health (NIH) Intellectual and Developmental Disabilities Research Centers Grant U54HD083092 (all cores) and a Shared Instrumentation Grant from the NIH (Grant 1S10OD016167 to the RNA In Situ and Microscopy Core) from the Eunice Kennedy Shriver National Institute of Child Health and Human Development. The content is the sole responsibility of the authors and does not necessarily represent the official views of the Eunice Kennedy Shriver National Institute of Child Health and Human Development or the NIH. This project was also funded by the Cancer Prevention and Research Institute Texas (Grant RP110390 to T.J.K.) and NIH Grants DC006185 and DC014832 to A.K.G., H.Y.Z. is an investigator of the Howard Hughes Medical Institute. We thank the members of the Zoghbi laboratory and Vicky Brandt for helpful discussions and comments on the manuscript and Rende Gu, Ph.D., for technical support on adult cochlear dissection.

The authors declare no competing financial interests.

Correspondence should be addressed to either of the following: Tiemo J. Klisch or Huda Y. Zoghbi, Department of Molecular and Human Genetics, Baylor College of Medicine, 1250 Moursund St. Ste. N1350, Houston, TX 77030. E-mail: hzoghbi@bcm.edu or klisch@bcm.edu.

DOI:10.1523/JNEUROSCI.0295-17.2017

 0270-6474/17/378583-12$15.00/0

regions of *Atoh1* (Mulvaney and Dabdoub, 2012; Groves et al., 2013), only a few studies have examined posttranslational modifications of Atoh1. Two recent studies identified phosphorylation sites that control Atoh1 stability in CGNs and inner ear hair cells through its interaction with Huwe1 (Forget et al., 2014; Cheng et al., 2016). In addition, serine 292 of the *Drosophila melanogaster* Atonal, a highly conserved phosphorylation site in the proneural protein classes of Ato, Ngn, and Achaete-Scute, was shown recently to enable precise spatiotemporal control of proneural activity in the fruit fly (Quan et al., 2016).

Our previous work showed that Atoh1 expression could induce ectopic chordotonal organs in wild-type flies and rescue chordotonal organ loss in *atonal* mutant fly embryos (Ben-Arie et al., 2000; Wang et al., 2002). We also showed that *atonal* could rescue the phenotype of *Atoh1*-null mice (Wang et al., 2002). To identify critical phosphorylation sites that mediate Atoh1 function during development, we reasoned that such sites would be evolutionarily conserved. The mouse Atoh1 protein has only one highly structured domain, the bHLH domain, which is 100% identical to human Atoh1 and 70% identical to the *Drosophila* atonal homolog (Cai et al., 2015a). Outside of this region, the Atoh1 peptide sequence diverges dramatically across species. Because it has been demonstrated that the bHLH domain conveys specificity to each bHLH transcription factor (Chien et al., 1996), we focused on phosphorylation sites within this domain.

We aligned fruit fly, frog, chicken, mouse, and human Atoh1 homologs and identified only one serine residue that could be phosphorylated, serine 193 (S193), the mouse analog to S292 in the fruit fly (see Fig. 1*A*). We showed previously that the phospho-mimetic S193D mutant loses the capability to bind to the AtEAM, the specific binding motif of Atoh1 (Klisch et al., 2011; Quan et al., 2016), resulting in a loss of transcriptional activity in an *in vitro* luciferase assay and an *in vivo* fly phenotype that was identical to that of *atonal*-null fruit flies (Quan et al., 2016). Because the phospho-mimetic was likely to phenocopy the *Atoh1*-null allele, we decided to generate a phospho-dead (serine to alanine) knock-in mouse model to investigate the *in vivo* function of S193.

Here, we show that S193 is phosphorylated *in vivo* and that an *Atoh1* allele carrying a mutation in this phosphorylation site results in specific neural, motor, and sensory deficits in mice, but at varying levels of severity. These findings highlight the differential sensitivity of certain cell types to Atoh1 function, suggesting that some are more vulnerable to disease resulting from partial Atoh1 dysfunction.

Materials and Methods

Generation of Atoh1-S193A *mice and genotyping*

We modified an *Atoh1-EGFP* tagged knock-in targeting construct (*pMath1EGFP_Neo*, Rose et al., 2009b) by mutating S193 to alanine (TCC → GCC) using the QuikChange Lightning Site-Directed Mutagenesis Kit (Agilent Technologies) with the following primer: 5′-CGAC AAGAAGCTGgCCAAATATGAGACCCTACAGATGGCCC-3′. Using albino C57BL/6 ES cells, we generated *Atoh1* $^{\text{Atoh1 - EGFP - S193A}}$ knock-in mice as described previously (Rose et al., 2009b) using the same genotyping primers (*Atoh1EGFP* forward: 5′-GCGATGATGGCACAGAAGG-3′; *Atoh1EGFP* reverse: 5′-GAAGGGCATTTGGTTGTCTCAG-3′). Figure 1 diagrams the genomic targeting strategy (Fig. 1*B*), confirmation of insertion locus by Southern blot (Fig. 1*C*), and PCR genotyping (Fig. 1*D*). The genotype was sequence verified by PCR amplification of *Atoh1* from homozygous knock-in mice. For simplicity, we refer to this allele *as Atoh1-S193A* throughout the text. *Atoh1-lacZ* control mice were genotyped using the primers and PCR protocol of the generic lacZ PCR from The Jackson Laboratory (transgene forward, oIMR3054: ATCCTCTG CATGGTCAGGTC; transgene reverse oIMR0040: CGTGGCCTGATTC ATTCC; internal control forward, oIMR8744: CAAATGTTGCTTGTCT GGTG; internal control reverse, oIMR8745: GTCAGTCGAGTGCA CAGTTT).

Mouse strains, husbandry, and handling

Animal housing, husbandry, and euthanasia were conducted under the guidelines of the Center for Comparative Medicine, Baylor College of Medicine. Mice were housed in an American Association for Laboratory Animal Science-certified Level 3 facility on a 14 h light cycle. After weaning, all mice were group housed (two to five mice per cage) as a mixture of genotypes. The investigators remained blind to the genotypes of all tested mice during phenotypic characterization and behavioral testing. Previously described mouse models are *Atoh1* lacZ (Ben-Arie et al., 2000), B6.129S7-Atoh1 $^{\text{tm2Hzo}}$/J (The Jackson Laboratory stock #005970), and Atoh1-GFP (Rose et al., 2009b, B6.129S-Atoh1 $^{\text{tm4.1Hzo}}$/J, #013593).

Behavior assays

The following assays have been described previously, but short descriptions are included below. All behavioral assays were performed with mice of both sexes.

Open-field assay (Chao et al., 2010). Mice were habituated for 30 min in the testing room (200-lux, 60 dB white noise), and then individually placed in the center of an open Plexiglas chamber (40 × 40 × 30 cm) with photo beams (Accuscan) to measure their activity. Data were analyzed by one-way ANOVA with Tukey's *post hoc* analysis.

Vertical rod assay (Matsuura et al., 1997). Mice were habituated for 30 min in the testing room and then placed individually on top of a 24-inch-tall wooden dowel and allowed to grip the dowel with all four paws. Latency to fall was recorded during the 2 min test. Data were analyzed by one-way ANOVA with Tukey's *post hoc* analysis.

Parallel rod foot-slip assay (Chao et al., 2010). Mice were habituated for 30 min in the testing room. Each mouse was placed in a foot-slip chamber consisting of a Plexiglas box with a floor of parallel rods and allowed to move freely for 10 min. Movement was recorded by a suspended digital camera and foot slips were recorded using ANY-maze software (Stoelting). The total number of foot slips was normalized to the distance traveled. Data were analyzed by one-way ANOVA with Tukey's *post hoc* analysis.

Rotarod assay (Chao et al., 2010). Mice were habituated for 30 min in the testing room, and then placed on a rotating cylinder of an accelerating rotarod apparatus (Ugo Basile) and allowed to move freely as rotation speed increased from 5 rpm to 40 rpm over a 10 min period. Latency to fall was recorded when the mouse fell from the rod or had ridden the rotating rod for three revolutions without regaining control. Four consecutive trials spaced at least 30 min apart were recorded in 1 d, and 4 consecutive days of trials were recorded. Data from all four trials were averaged per day and analyzed by two-way ANOVA with Tukey's *post hoc* analysis.

Unrestrained whole-body plethysmography (UWBP) (Huang et al., 2012). Mice were placed within air-flushing UWBP chambers (Buxco) with a flow rate of 0.5 L/min. Respiratory parameters were captured using Ponemah 3 software (DSI) and processed using MATLAB (The MathWorks, RRID: SCR_001622). Mice were allowed to acclimate for at least 20 min and baseline breathing was recorded for at least 20 min. To determine response to hypercapnia gas, the chamber was flushed with hypercapnic gas (5% CO_2) for 15 min, breathing was recorded for the first 5 min of hypercapnic exposure, and mice were allowed to recover in fresh air for 15 min. Hypoxic gas (10% O_2) challenge was done in the same manner. Data were analyzed by two-way ANOVA with Tukey's *post hoc* analysis.

Auditory brainstem response (ABR) recording (Cai et al., 2013). Mice were anesthetized using an intraperitoneal injection of ketamine (100 mg/kg) and xylazine (10 mg/kg) and immobilized in a head holder. Pure tone stimuli from 4 kHz to 48 kHz were generated using Tucker Davis Technologies System 3 digital signal processing hardware and software (RRID: SCR_014520) and the intensity of the tone stimuli was calibrated using a type 4938, 1/4-inch pressure-field calibration microphone (Brüel and Kjær). Response signals were recorded with subcutaneous needle electrodes inserted at the vertex of the scalp, the postauricular region (reference), and the back leg (ground). Auditory thresholds were determined by decreasing the sound intensity of each stimulus from 90 dB to 10 dB in 5 dB steps until the lowest sound intensity with reproducible

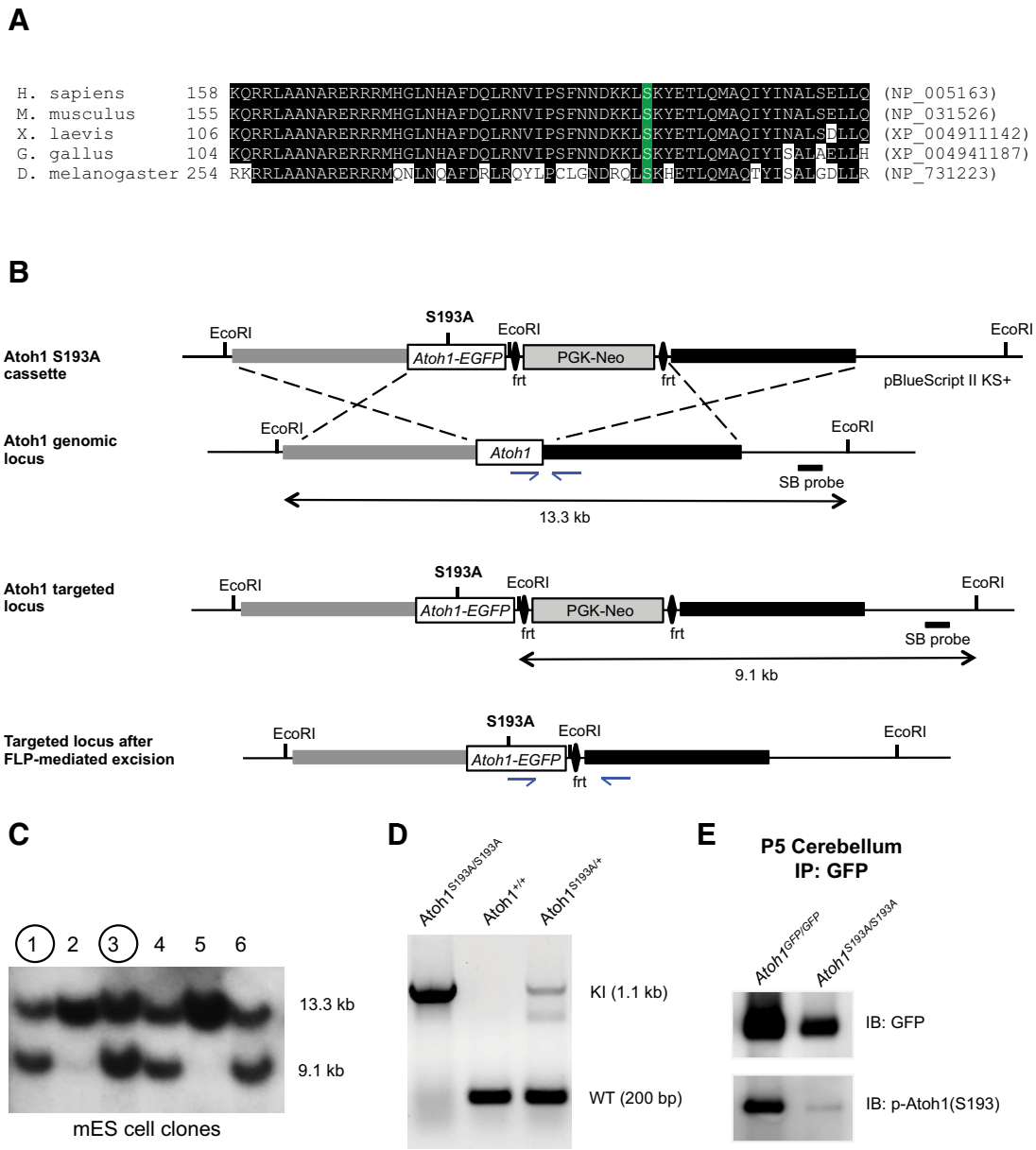

Figure 1. S193 is a highly conserved phosphorylation site in Atoh1. ***A***, Alignment of bHLH domain sequences between *H. sapiens* (human, NP_005163), *M. musculus* (mouse, NP_031526), *G. gallus* (chicken, XP_004941187), *X. laevis* (frog, XP_004911142), and *D. melanogaster* (fly, NP_731223). S193 is marked white on green. Numbers indicate position of bHLH domain in protein sequence. Identical amino acids are white on black. ***B***, Targeting schematic of *Atoh1-S193A* allele. S193 is mutated to an alanine in a targeting construct that contains an *EGFP* coding sequence fused to the 3′ end of the *Atoh1* coding sequence. Together with an frt-flanked PGK-Neo selection cassette, the mutated *Atoh1-EGFP* coding sequence is placed between intact *Atoh1* 5′ and 3′ homology arms. This construct was targeted to the *Atoh1* genomic locus, followed by subsequent removal of the PGK-Neo cassette as depicted. ***C***, EcoRI-digested genomic DNA from six mouse embryonic stem cell clones show that four of six carry the targeted allele when probed with a DNA probe that lies outside of the homology arms. Two clones (1 and 3) were selected for mouse blastocyst injection. ***D***, PCR genotyping of WT, *Atoh1*$^{S193A/+}$, and *Atoh1*$^{S193A/S193A}$ mice. ***E***, S193 is phosphorylated *in vivo*. EGFP-tagged Atoh1 was immunoprecipitated from P5 cerebella of *Atoh1*$^{GFP/GFP}$ and *Atoh1*$^{S193A/S193A}$ mice and immunoblotted with GFP antibody or the generated phospho-specific antibody to S193, pAtoh1(S193).

and recognizable waves in the response was reached. Peak amplitude and latency were measured using BioSig software from Tucker Davis Technologies. Mean absolute hearing thresholds ± SDs (decibels SPL) were plotted as a function of stimulus frequency (in kilohertz) for each genotype. Statistical analysis consisted of one-way ANOVA to reveal overall trends accompanied by two-tailed Student's *t* tests at individual frequencies or intensities with adjustment of *p*-values for multiple comparisons using the Tukey's HSD method. R (version 3.2.4, R Project for Statistical Computing, RRID: SCR_001905) was used for all statistical analyses.

Statistical analyses

Statistical significances were tested using ANOVA (one-way and two-way as appropriate) with Tukey's *post hoc* analysis using Prism 6 (GraphPad, RRID: SCR_002798) for all analyses except for ABR data, which was analyzed with R (version 3.2.4, R Project for Statistical Computing, RRID: SCR_001905). Specific *p*-values are reported in Table 1.

X-gal staining and Nissl staining

Whole-mount X-gal staining was performed as described previously using 1 mg/ml Bluo-Gal (Invitrogen; Huang et al., 2012). After fixation and X-gal staining, inner ears were dissected and dehydrated in an ethanol gradient (1 h in 30% ethanol, 1 h in 50% ethanol, overnight in 95% ethanol, and overnight in 100% ethanol at room temperature). Inner ears were cleared in methyl salicylate overnight at room temperature. Nissl staining was performed as described previously (Flora et al., 2007).

Table 1. Statistical analyses of behavioral data

Figure	Definition of population	Population size (*n*)	Comparison[a]	*p*-value
2B	Individual mice	12–15	WT vs S193A/lacZ, Day 3	0.0053
			WT vs S193A/lacZ, Day 4	0.0012
2C	Individual mice	3	WT vs 193A/lacZ	0.0380
4A	Individual mice	6	WT vs S193A/+	0.0010
			WT vs S193A/S193A	0.00012
			WT vs S193A/lacZ	1.40_E-11
			lacZ/+ vs S193A/lacZ	0.000014
			S193A/S193A vs S193A/lacZ	0.014
4C	Individual mice, per time point	4–5	P0 lacZ/+ vs S193A/lacZ, inner apex	0.0129
			P0 lacZ/+ vs S193A/lacZ, inner mid	0.0015
			P0 lacZ/+ vs S193A/lacZ, inner base	0.0006
			P0 lacZ/+ vs S193A/lacZ, outer apex	<0.0001[b]
			P0 lacZ/+ vs S193A/lacZ, outer mid	0.0595
			P0 lacZ/+ vs S193A/lacZ, outer base	<0.0001[b]
			P5 lacZ/+ vs S193A/lacZ, inner apex	0.0014
			P5 lacZ/+ vs S193A/lacZ, inner mid	<0.0001[b]
			P5 lacZ/+ vs S193A/lacZ, inner base	0.0053
			P5 lacZ/+ vs S193A/lacZ, outer apex	<0.0001[b]
			P5 lacZ/+ vs S193A/lacZ, outer mid	<0.0001[b]
			P5 lacZ/+ vs S193A/lacZ, outer base	0.0007
			P21 lacZ/+ vs S193A/lacZ, outer apex	0.0013
			P21 lacZ/+ vs S193A/lacZ, outer mid	<0.0001[b]
			P21 lacZ/+ vs S193A/lacZ, outer base	<0.0001[b]
			P5 lacZ/+ vs S193A/S193A, outer apex	0.0477
			P21 lacZ/+ vs S193A/S193A, outer base	0.0112
5B	Individual mice	3	lacZ/+ vs S193A/lacZ, circumference	0.0011
6D	Individual mice	5	Scn11a, WT vs S193A/S193A	<0.0001[b]
			Scn11a, WT vs S193A/lacZ	<0.0001[b]
			Mgat5b, WT vs S193A/S193A	0.0483
			Mgat5b, WT vs S193A/lacZ	0.0222
			Rasd2, WT vs S193A/lacZ	0.0131
			Rbm24, WT vs S193A/lacZ	0.0208

[a]Only significant values are listed.

[b]Prism 6 only reports up to four decimal points.

Cochlea isolation and sectioning

Heads from postnatal day 0 (P0) and P5 mice were fixed with 4% paraformaldehyde for 3 h at room temperature. Embryonic day 16.5 (E16.5) embryos were fixed in 4% paraformaldehyde for 30 min. Heads were washed and stored in PBS at 4°C. Cochleae or utricles were dissected in PBS after fixation. To obtain P21 and adult cochlea, whole-body perfusion was performed and the inner ears were dissected and postfixed in 4% paraformaldehyde overnight at 4°C. Cochleae or utricles were dissected in PBS and decalcified in 500 mM EDTA overnight at 4°C. For cochlear section staining, mouse heads were fixed for 3 h in 4% paraformaldehyde at room temperature, washed with PBS, and cryoprotected in 30% sucrose in PBS at 4°C until they sank. The cryoprotected heads were then embedded in optimal cutting temperature medium and sectioned at 14 μm.

Immunohistochemistry

Primary antibodies used in this study were anti-activated Caspase 3 (act-Casp3, 1:500, rabbit; R & D Systems catalog #AF835, RRID: AB2243952), anti-Myosin7 (1:500, rabbit; Proteus Biosciences catalog #25-6790, RRID: AB_2314839), and anti-p27kip1 (1:250, mouse; Thermo Fisher Scientific catalog #MA5-12835, RRID: AB_10988513). Secondary antibodies were anti-mouse Alexa Fluor 488 (1:2000, goat; Thermo Fisher Scientific catalog #A-11029, RRID: AB_2534088) or anti-rabbit Alexa 594 (1:2000, goat; Thermo Fisher Scientific catalog #R37117, RRID: AB_2556545). Cell nuclei were labeled by DAPI (1:10,000; Thermo Fisher Scientific catalog #D1306, RRID: AB_2629482). The immunostaining procedure followed standard protocol using 0.1% Triton X-100 in PBS washes and 10% goat serum in the primary antibody blocking buffer.

Quantitative PCR

The temporal bone containing the inner ear was dissected from P0 mice and placed into 1 ml of TRIzol (Thermo Fisher Scientific) and the recommended protocol by the manufacturer was followed to isolate RNA. First-strand cDNA was synthesized using M-MLV reverse transcriptase (Thermo Fisher Scientific). Quantitative RT-PCR was performed using 2× SYBR green reaction mixture and the Bio-Rad CFX96 Real-Time system. The target gene primer sets were either chosen from Primerbank (Wang et al., 2012) or designed using Primer 3 Plus (Untergasser et al., 2007). The following primers were used: *Anxa4*: forward 5′-CAAAGG AGGAACCGTGAAAGC-3′, reverse 5′-GCATCTTCATCAGTACCGA GG-3′; *Atoh1*; forward 5′-CAACGACAAGAAGCTGTCCA-3′, reverse 5′-GAGTAACCCCCAGAGGAAGC-3′; *Mgat5b*: forward 5′-GAGACCCTT TCGGCTGTTTGT-3′, reverse 5′-CCAGCATATCCATGCGCTTC-3′; *Mreg*: forward 5′-GTGGTAACAATCCGTATTCCTCC-3′, reverse 5′-TCCTCTAAGATTCGTCTCCATCG-3′; *Rasd2*: forward 5′-AACTGCG CCTACTTCGAGG-3′, reverse 5′-GGTGAAAAGCATCGCCGTACT-3′; *Rbm24*: forward 5′-GGGGCTACGGATTTGTCACC-3′, reverse 5′-TG GCTGCATGATTCTTGGTTT-3′; *Scn11a*: forward 5′-CGACTCTT TGGCTGCAATAGA-3′, reverse 5′-AGAGCTTAGGTAACTTCCTGGAG-3′.

Western blot analysis

Protein lysates were prepared from cerebella of P5 mouse pups by trituration in lysis buffer (50 mM Tris, pH 7.5, 150 mM NaCl, 1 mM EDTA, 0.5% Triton X-100, 1 mM PMSF; Roche Complete Protease Inhibitor) with 1 ml syringes and 23G needles followed by 29G1/2 needles. Samples were sonicated and rotated for 10 min at 4°C. After centrifugation at 13,000 rpm for 10 min, the supernatant was mixed with 2× NuPAGE sample buffer and run on a NuPAGE 4–12% Bis-Tris gradient gel in MES Running Buffer (Thermo Fisher Scientific). Proteins were transferred to nitrocellulose membranes using the MES NuPAGE transfer system for 1 h at 4°C. The membranes were blocked with 5% BSA in TBS with 0.1% Tween 20 (TBST) and incubated with primary antibody overnight at 4°C with mild agitation. After washing with TBST, the membranes were incubated with secondary antibody for 1 h at room temperature followed by washing. HRP was detected using the Pierce ECL detection kit. Antibodies used were as follows: polyclonal anti-pAtoh1(S193) (1:2000, rabbit; GenScript), polyclonal anti-GFP (1:5000, rabbit; GeneTex catalog #GTX113617, RRID: AB_1950371), monoclonal anti-vinculin (1:5000, mouse; Millipore catalog #MAB3574, RRID: AB_2304338), HRP-conjugated anti-rabbit IgG (1:20,000, donkey; GE Healthcare catalog #RPN4301, RRID: AB_2650489), and HRP-conjugated anti-mouse IgG (1:20,000, donkey; Jackson ImmunoResearch Laboratories catalog #715-035-150, RRID: AB_2340770).

Cycloheximide assay

DAOY cells (ATCC catalog #HTB-186, RRID: CVCL_1167) were transfected using Lipofectamine LTX and Plus reagents with a ratio of Plus-DNA-LTX of 1 μl to 1 μg to 3 μl (Thermo Fisher Scientific) per the manufacturer's instructions. For each sample (1.25×10^5 cells), 250 ng of *pcDNA3_Atoh1-GFP* constructs were transfected. After 24 h, cycloheximide was added to cell media to a final concentration of 10 μg/ml. Cell lysates were collected at five time points after exposure to cycloheximide: 0, 2, 4, 6, and 8 h. Western blot images were processed and quantified with ImageJ (RRID: SCR_003070) with each lane normalized to the loading control. The experiment was repeated six times.

Chromatin immunoprecipitation (ChIP)

Cochlea were dissected from P0 *Atoh1*$^{GFP/GFP}$ and *Atoh1*$^{S193A/193A}$ pups and stored in DMEM with 5% FBS. Eight cochlea were collected for each sample and centrifuged at 470 × *g* for 10 min at 4°C. DMEM was carefully removed and samples were cross-linked in 500 μl of PBS containing 1% formaldehyde (VWR) for 20 min at room temperature in a tail-over-head rotator. Fixation was quenched with 0.25 M glycine. Cross-linked tissue was centrifuged at 470 × *g* for 10 min at 4°C. The supernatant was removed and the pellet was washed with 500 μl of ice-cold PBS three times. After removal of final PBS wash, samples were snap frozen in liquid nitrogen and stored at −80°C. ChIP was performed as described previously (Cai et al., 2015b). The following primers were used for quantitative PCR after ChIP: *Atoh1*: forward

5′-CCAAGAAGCGTGGGGGTAG-3′, reverse 5′-GCTTCTGTAAACT CTGCCGG-3′; *Anxa4*: forward 5′-CTTTTACCTGCCCCGCCCA-3′, reverse 5′-GAAACGGCACCTGACCTGTTA-3′; *Fgf18:* forward 5′-TGTTCTAGCCCCATCAGCTT-3′, reverse 5′-GCTTGCACTACATG GCTCTG-3′; *Mgat5b*: forward 5′-GGCTGCTGTCTCTGTCTTGT-3′, reverse 5′-CCTCGAAGCCTGGAGAAGTC-3′; *Mreg*: forward 5′-CCT CCTCTGGTCTCTGGGTG-3′, reverse 5′-TTCCTGTGCATAGTCGC CTG-3′; *Rasd2*: forward 5′-GGCACAAAAGATGCACAGGG-3′, reverse 5′-GCAGCCTCCAAGTGTTCAA-3′; *Rbm24*: forward 5′-GCTACTAA GCAGAAGGGACGG-3′, reverse 5′-ATCGAGTGGCTTAGTGGGAT-3′; *Scn11a*: forward 5′-CCTGCAGTTTGCACCTTTCC-3′, reverse 5′-GGG CAGGAGAGAAGAAACCC-3′.

Results

S193 of Atoh1 is highly conserved and phosphorylated *in vivo*

As noted above, we identified only one serine residue in the bHLH domain that could be phosphorylated, S193 (Fig. 1*A*). Because the phospho-mimetic (serine to aspartic acid, S193D) mutant was functionally null in the fruit fly (Quan et al., 2016) and thus likely to phenocopy the *Atoh1*-null allele, we decided to generate a phospho-dead (serine to alanine, S193A) knock-in mouse model to investigate the *in vivo* function of S193 (Fig. 1*B–D*).

To determine whether S193 is phosphorylated *in vivo*, we generated a phospho-specific antibody that recognizes pAtoh1(S193). To test its specificity, we immunoprecipitated Atoh1 from P5 cerebellar lysates of *Atoh1*$^{\text{Atoh1 - GFP/Atoh1 - GFP}}$ (Rose et al., 2009b) and our *Atoh1*$^{\text{Atoh1 - GFP - S193A/Atoh1 - GFP - S193A}}$ mice—from here on abbreviated as *Atoh1*$^{\text{GFP/GFP}}$ and *Atoh1*$^{\text{S193A/S193A}}$, respectively—using the GFP tag and immunoblotted using GFP antibodies for total Atoh1 protein and our pAtoh1(S193) antibody (Fig. 1*E*). The much weaker pAtoh1(S193) immunoreactivity from the homozygous knock-in mice indicates that our antibody is specific, whereas the immunoreactivity in the wild-type mice indicates that S193 is indeed phosphorylated *in vivo*.

Atoh1$^{\text{S193A/lacZ}}$ mice have motor coordination deficits and cerebellar foliation defects

Because *Atoh1* heterozygosity is sufficient for normal cerebellar development and our homozygous *Atoh1*$^{\text{S193A/S193A}}$ mice did not show the postnatal lethality phenotype of the *Atoh1*-null allele, we suspected that the phospho-mutant phenotype is milder than the null allele. Indeed, we showed previously that the phospho-dead (S193A) mutant loses neither DNA-binding capacity nor significant transcriptional activity in a luciferase reporter assay (Quan et al., 2016). Nevertheless, the *in vivo* Atonal phospho-dead (S292A) fly mutant did exhibit mild loss-of-function phenotypes, specifically smaller and disorganized ommatidia (Quan et al., 2016). We therefore generated another cohort of *Atoh1-S193A* mice on an *Atoh1*-null background (*Atoh1*$^{\text{S193A/lacZ}}$; Ben-Arie et al., 2000).

Mice carrying the S193A allele on either wild-type or null backgrounds were born at the expected Mendelian ratios, their body weights were similar to those of control cohorts (*Atoh1*$^{\text{WT}}$ and *Atoh1*$^{\text{lacZ/+}}$), and no irregular movements or behavior were detected when observing the mice in their home cages. Because Atoh1 plays an important role in proprioception and interoception (Rose et al., 2009a), we decided to assess their motor coordination in more detail. No difference was detected between the phospho-mutant mice and control littermates in the open-field assay for general locomotor activity, vertical rod assay for sensorimotor impairment, or parallel rod foot-slip assay for ataxia ($n = 7–9$; Fig. 2*A*), but *Atoh1*$^{\text{193A/lacZ}}$ mice performed significantly worse than control littermates on days 3 and 4 of an accelerating rotarod assay ($n = 12–15$, day 3: $^*p = 0.0053$, day 4: $^*p = 0.0012$, two-way ANOVA; Fig. 2*B*). To determine the underlying anatomical basis of this motor coordination or motor learning deficit, we performed Nissl staining on adult mouse cerebella and found that *Atoh1*$^{\text{S193A/lacZ}}$ mice have decreased foliation between lobules VI and VII as assessed by the area of the molecular layer of both lobules (outlined in pink in Fig. 2*C*, $n = 3$, $^*p = 0.0356$, ANOVA).

Atoh1$^{\text{193A/lacZ}}$ mice have a pontine neuronal progenitor migration defect

Atoh1 defines the rhombic lip and its lineages, which give rise to numerous nuclei responsible for the proprioceptive, vestibular, auditory, and respiratory systems in the hindbrain (Rose et al., 2009a,b). Therefore, we tested respiration of the *Atoh1-S193A* phospho-mutant mice using unrestrained whole-body plethysmography (UWBP) and found no difference in baseline breathing or hypoxic and hypercapnic respiration stress tests (Fig. 3*A*). We concluded that Atoh1-positive neurons that regulate respiration were intact and functional.

To determine whether the other Atoh1-positive nuclei were affected, we evaluated β-gal expression in E16.5 hindbrains of *Atoh1*$^{\text{lacZ/+}}$ and *Atoh1*$^{\text{S193A/lacZ}}$ embryos. Serial coronal sections through the brainstem revealed that these nuclei are intact in the E16.5 *Atoh1*$^{\text{S193A/lacZ}}$ embryos, suggesting that S193 phosphorylation is not required for the initial generation of these rhombic lip-derived, Atoh1-positive nuclei (Fig. 3*B*). We also evaluated β-gal expression in postnatal day 0 (P0) mice. Interestingly, there was a partial defect in pontine neuronal migration as shown by the continued presence of the anterior extramural migratory stream in the *Atoh1*$^{\text{S193A/lacZ}}$ mice (Fig. 3*C*). This delay in migration was not apparent at E16.5 because pontine neuronal progenitor migration is ongoing and incomplete at that stage. These findings suggest that, whereas the majority of Atoh1-dependent neuronal progenitors are unaffected in *Atoh1*$^{\text{S193A/lacZ}}$ mice, the migration of pontine nucleus progenitors is partially affected.

Atoh1-S193A phospho-mutant mice are deaf and progressively lose inner ear hair cells

The mechanosensory hair cells of the inner ear are dependent on Atoh1 expression for proper development and survival (Bermingham et al., 1999; Cai et al., 2013). To investigate whether these Atoh1-dependent cells were affected in our *Atoh1-S193A* phospho-mutant mice, we performed auditory brainstem response (ABR) tests to assess hearing in adult mice. *Atoh1*$^{\text{S193A/lacZ}}$ mice were profoundly deaf by 2 months of age ($n = 6$, $^*p = 2.13\text{e-}10$, two-way ANOVA; Fig. 4*A*, red). *Atoh1*$^{\text{S193A/S193A}}$ mice exhibited a milder hearing loss, with decreased ABR thresholds at frequencies >12 kHz (Fig. 4*A*). To our surprise, 2-month-old *Atoh1*$^{\text{lacZ/+}}$ mice, which had previously been thought to show no effects of heterozygosity (Ben-Arie et al., 1997; Fritzsch et al., 2005; Wang et al., 2005), also exhibited loss of hearing at frequencies >20 kHz (Fig. 4*A*). We then analyzed whole-mount preparations of the cochlea stained for Myosin VIIa of these ABR-tested mice. We discovered hair cell degeneration in the *Atoh1*$^{\text{S193A/lacZ}}$, *Atoh1*$^{\text{S193A/S193A}}$, and *Atoh1*$^{\text{lacZ/+}}$ mice that were commensurate with the level of hearing loss revealed in the ABR tests (Fig. 4*B*).

We next investigated how early the hair cell degeneration begins by examining a series of whole-mount cochlea at the P0, P5, and P21 time points and observed a progressive loss of cochlear hair cells for *Atoh1*$^{\text{S193A/lacZ}}$ and *Atoh1*$^{\text{S193A/S193A}}$ mice (Fig. 4*C*). As expected, *Atoh1*$^{\text{S193A/lacZ}}$ mice exhibited the earliest degeneration, which was already evident at P0. *Atoh1*$^{\text{S193A/S193A}}$ mice, which had an intermediate hearing loss phenotype, did not begin to exhibit

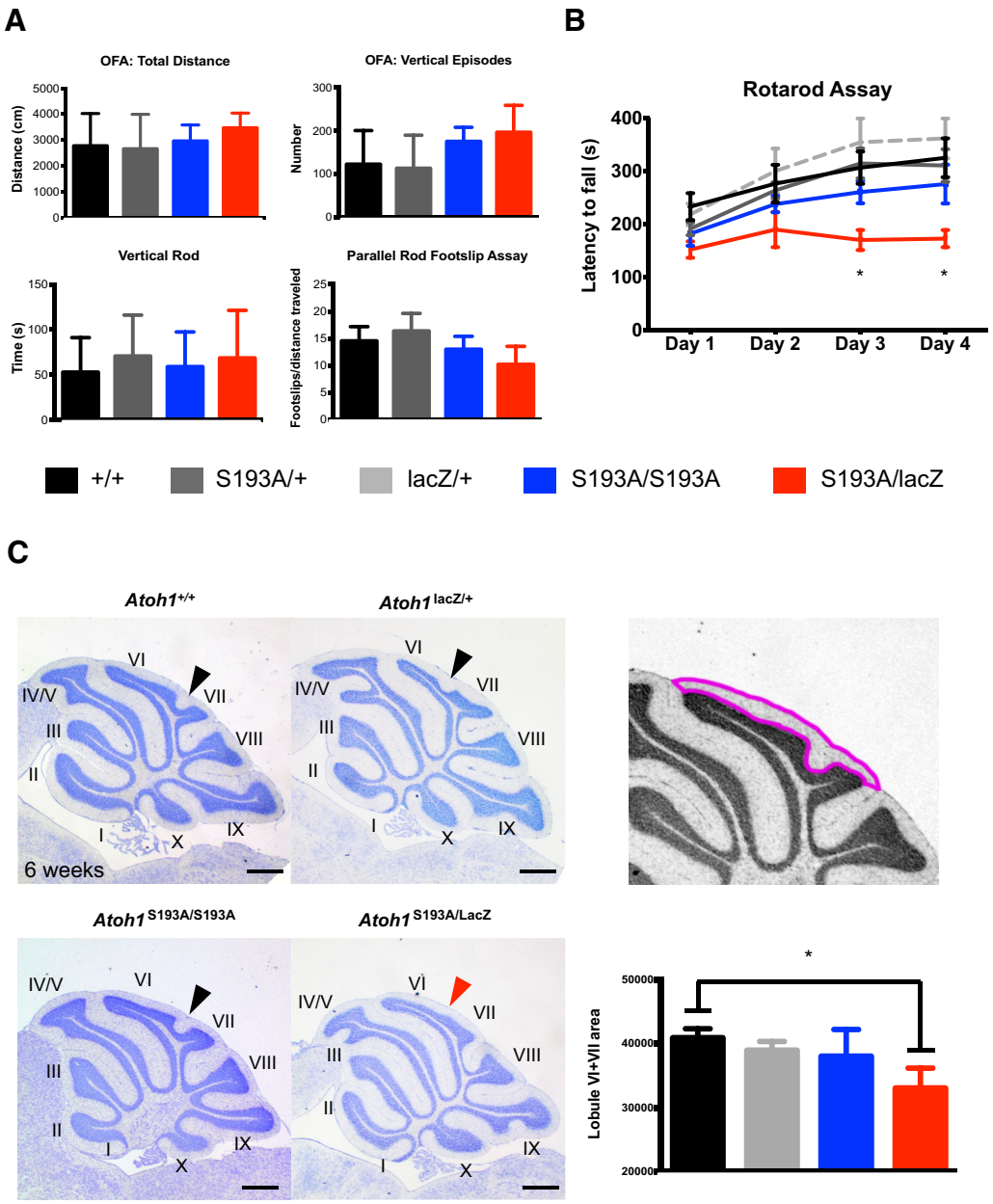

Figure 2. *Atoh1*$^{S193A/lacZ}$ mice perform poorly on the rotarod and have a foliation defect in the cerebellum. ***A***, Behavioral data showing total distance traveled and number of vertical episodes in the open field assay, total time spent in the vertical rod assay, and number of foot slips per distance traveled in the parallel rod foot-slip assay ($n = 7–9$, 2-month-old mice). Shown are mean values ± SEM; there was no statistical significance. ***B***, Latency to fall on the accelerating rotarod over the course of 4 d with 4 trials per day ($n = 12–15$). Shown are mean values ± SEM. Day 3: $*p = 0.0053$, day 4: $*p = 0.0012$, two-way ANOVA. ***C***, Sagittal sections of 6-week-old mouse cerebella near the midline. Black arrowheads point to foliation between lobules VI and VII. Red arrowhead points to missing foliation between lobules VI and VII in *Atoh1*$^{S193A/lacZ}$ mice. Cerebellar lobule area was calculated using ImageJ to outline the molecular layer of lobules VI and VII ($n = 3$). Scale bar, 1 mm. Data are shown as mean ± SEM. $*p = 0.0356$, one-way ANOVA.

hair cell loss until P21, and *Atoh1*$^{lacZ/+}$ mice were indistinguishable from wild-type mice at these early time points (Fig. 4*C*).

Atoh1$^{193A/lacZ}$ mice lose cochlear hair cells as early as E16.5

Atoh1-null mice show cochlear hair cell death as early as E15.5 (Chen et al., 2002; Pan et al., 2011; Cai et al., 2013). To determine whether *Atoh1*$^{193A/lacZ}$ mice fail to specify hair cells or lose them via cell death, we performed whole-mount cochlear staining using an anti-activated Caspase 3 antibody (ActCasp3) to mark apoptotic cells. *Atoh1*$^{S193A/lacZ}$ mouse cochleae show ActCasp3 staining, indicating that the hair cell loss is due to apoptosis during development (Fig. 5*A*). The similarity to the phenotype of *Atoh1*-null mice also suggests that the hair cell loss arises from loss of Atoh1 function.

Atoh1-S193A phospho-mutant mice do not show hair cell loss in the vestibular system

Because impaired vestibular function can also contribute to a poor rotarod performance, we investigated the hair cells of the vestibular system (Gnedeva and Hudspeth, 2015; Haque et al., 2016). To determine the size and hair cell density of the macula and cristae, we performed immunostaining with Myosin VIIa. We found that both the maculae and cristae of adult *Atoh1*$^{S193A/S193A}$ and *Atoh1*$^{S193A/lacZ}$ mice were normal in size and hair cell density

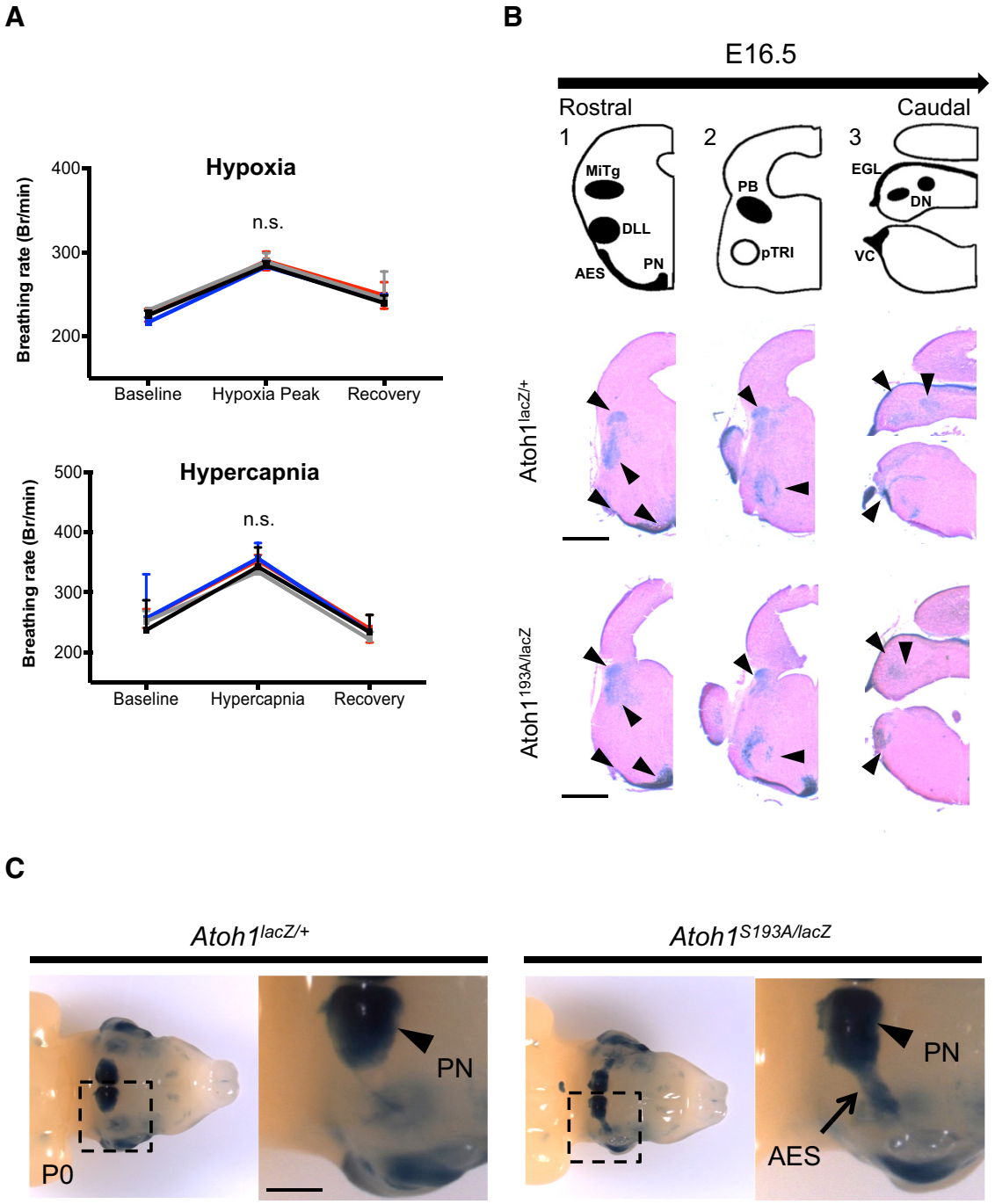

Figure 3. *Atoh1*$^{S193A/lacZ}$ mice have a pontine nucleus migration defect. ***A***, Unrestrained whole-body plethysmography of 2-month-old mice ($n = 4$). Graphs show no change in respiratory frequency (breaths per minute, Br/min) when challenged with hypoxia (10% O_2) or hypercapnia (5% CO_2). Data are shown as mean ± SEM over 20 min of normoxic baseline, 5 min of gas challenge, and 15 min of normoxic recovery. ***B***, Serial coronal sections from E16.5 *Atoh1*$^{lacZ/+}$ and *Atoh1*$^{S193A/lacZ}$ brainstems at approximate levels 1–3. DLL, Dorsal lateral lemniscal; DN, deep cerebellar nuclei; EGL, external granule layer; MiTg, microcellular tegmental; PB, parabrachial; PN, pontine nuclei; pTRI, paratrigeminal; VC, ventral cochlear. All nuclei are present. Scale bar, 500 μm. ***C***, Ventral view of whole-mount β-galactosidase staining of three P0 *Atoh1*$^{lacZ/+}$ and *Atoh1*$^{S193A/lacZ}$ hindbrains. Arrowhead points to the pontine nucleus (PN) and the arrow points to the anterior migratory stream (AES), which is affected in the *Atoh1*$^{S193A/lacZ}$ mutants.

(Fig. 5*B*), suggesting that impaired vestibular function is not a contributing factor to the poor rotarod performance seen in the *Atoh1*$^{S193A/lacZ}$ mice.

Misregulation of Atoh1 target genes in *Atoh1*$^{S193A/lacZ}$ hair cells

To investigate the mechanism by which the *Atoh1-S193A* phospho-mutant causes hair cell loss, we first investigated whether the levels of Atoh1 RNA or protein was affected in *Atoh1*$^{S193A/lacZ}$ mice. Atoh1 RNA levels from the inner ear of *Atoh1*$^{S193A/S193A}$ mice and *Atoh1*$^{S193A/lacZ}$ mice were similar to those of littermate controls (Fig. 6*A*). Using an antibody to the GFP tag, we found that Atoh1 protein levels were unchanged in *Atoh1*$^{S193A/S193A}$ mouse cerebella compared with cerebella of *Atoh1*$^{GFP/GFP}$ control mice, suggesting that phosphorylation of S193 does not play a role in regulating Atoh1 protein levels (Fig.

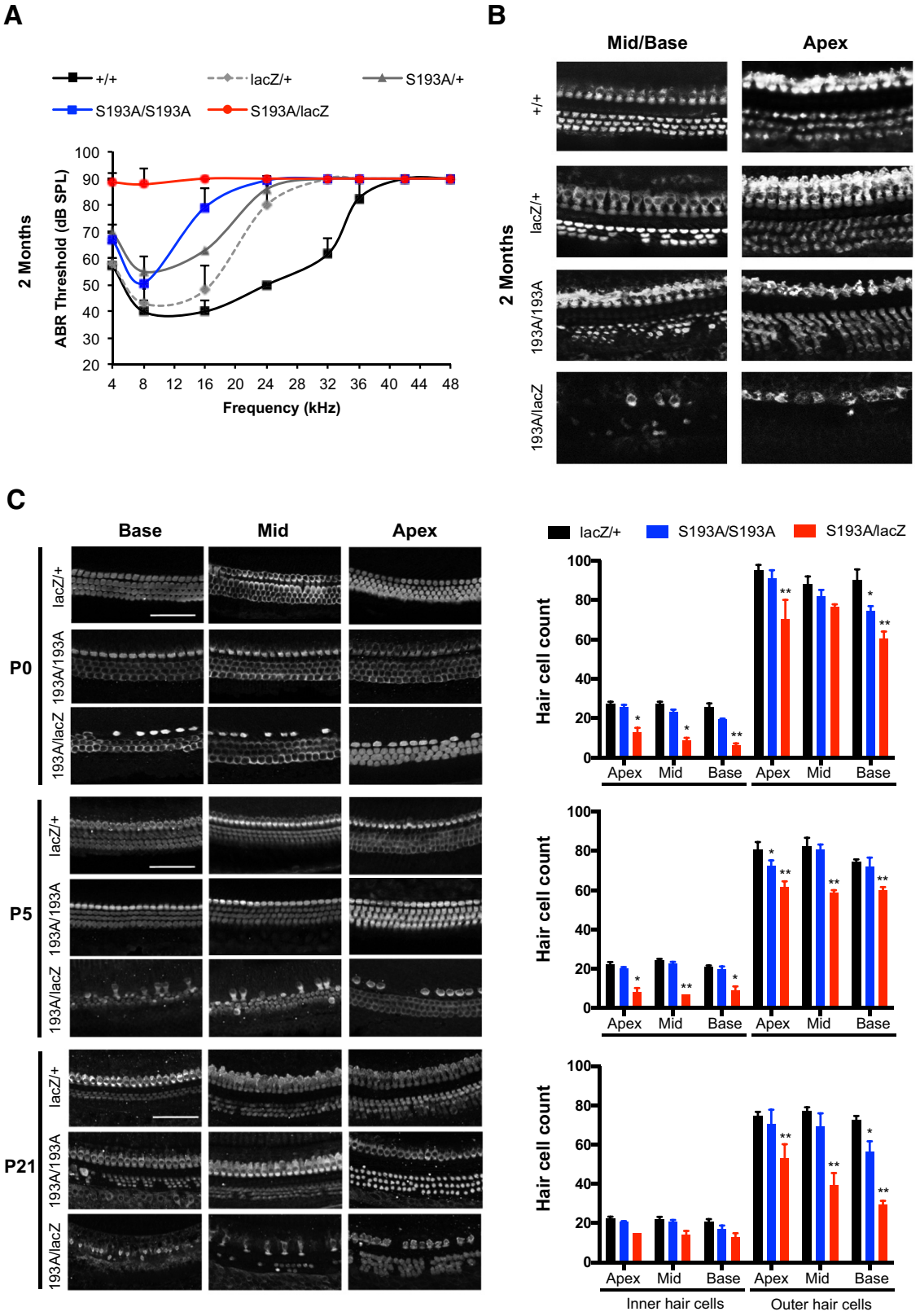

Figure 4. *Atoh1*$^{S193A/lacZ}$ mice have accelerated hearing loss due to progressive inner ear hair cell loss. ***A***, ABR assay of 2-month-old mice. *Atoh1*$^{193A/lacZ}$ mice are profoundly deaf and *Atoh1*$^{193A/193A}$ mice have hearing loss at frequencies over 12 kHz. Data are shown as mean ± SEM. ***B***, Whole-mount cochlear staining of 2-month-old mice with Myosin VIIa. Hair cell degeneration is shown in *Atoh1*$^{S193A/lacZ}$, *Atoh1*$^{193A/193A}$ and *Atoh1*$^{lacZ/+}$ mice, with degeneration being most severe in the *Atoh1*$^{S193A/lacZ}$ mice. Scale bar, 20 μm. ***C***, Different regions of whole-mount cochlea at three postnatal time points: P0, P5, and P21. Numbers of inner and outer hair cells were quantified and shown in graphs to the right. Loss of inner ear hair cells is apparent in both *Atoh1*$^{193A/193A}$ and *Atoh1*$^{193A/lacZ}$ mice ($n = 3$), with the latter being more severe. Hair cells were counted per 200 μm length. Data are shown as mean ± SEM. *$p < 0.01$, **$p < 0.001$, one-way ANOVA. Scale bar, 20 μm.

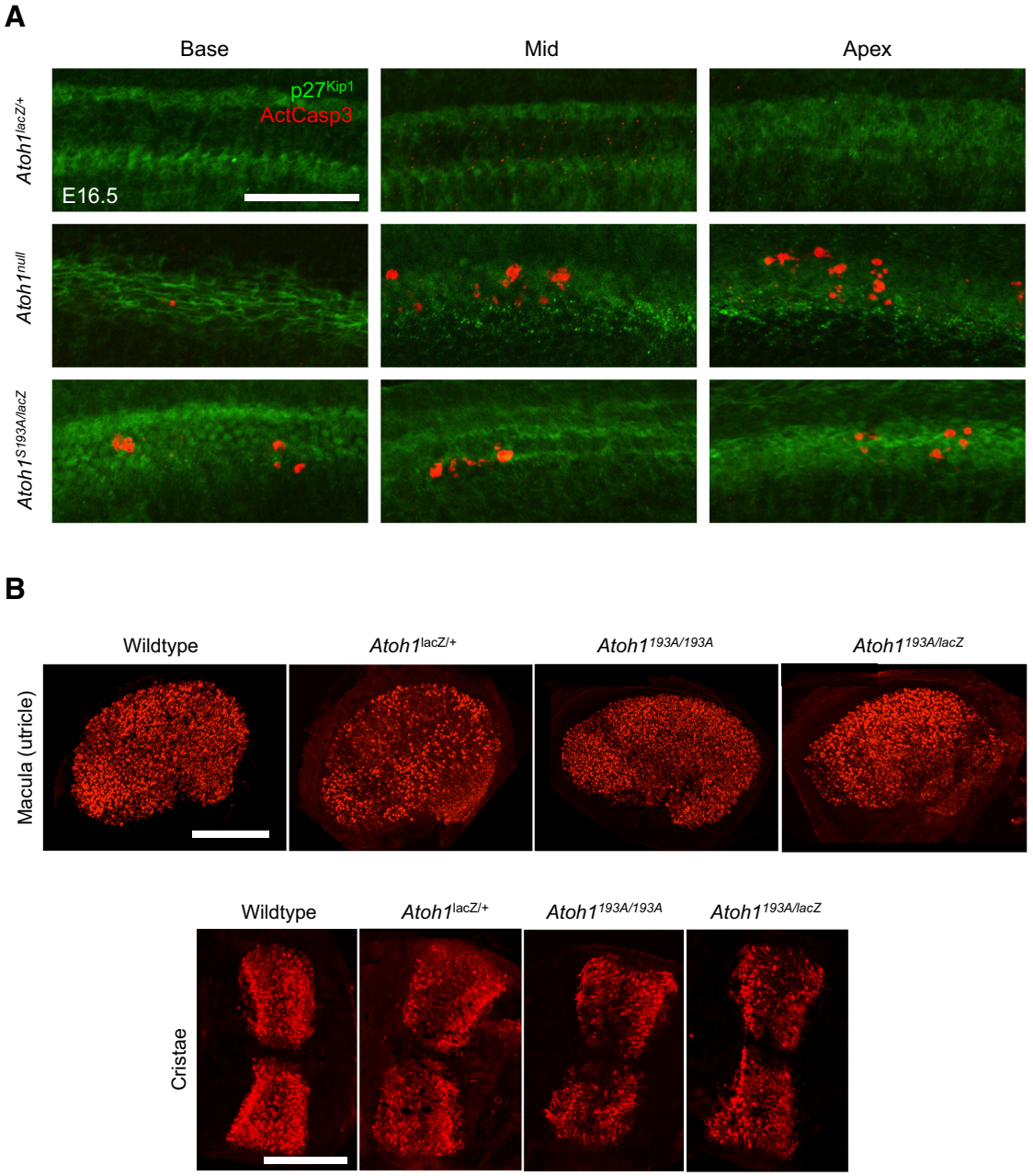

Figure 5. Caspase3 signal is seen as early as E16.5 in *Atoh1*$^{S193A/lacZ}$ mice. ***A***, Immunofluorescence of whole-mount cochlea from E16.5 mice. p27^{kip1} (green) marks the prosensory epithelia. ActCasp3 (red) marks apoptotic cells. Scale bar, 20 μm. ***B***, Whole-mount staining with Myosin VIIa of utricles and cristae from 2-month-old mice. Scale bar, 200 μm.

6*B*). To confirm that S193 does not affect protein stability, we performed a cycloheximide pulse-chase assay to measure the protein half-life of both phospho-mimetic and phospho-dead S193 Atoh1 mutants in medulloblastoma DAOY cells. We found no difference between the half-life of the phospho-mutant and the wild-type proteins (Fig. 6*C*). We thus concluded that the *Atoh1-S193A* mutation does not alter Atoh1 half-life or play a role in Atoh1 protein degradation.

Next, we investigated the expression levels of previously validated Atoh1 direct target genes in the inner ear (Cai et al., 2015b). We found that some genes had altered expression levels, whereas others were unaffected (Fig. 6*D*). *Anxa4* and *Mreg* gene expression were not changed significantly, whereas *Scn11a*, *Mgat5b*, *Rasd2*, and *Rbm24* were downregulated in *Atoh1*$^{S193A/lacZ}$ mice and only *Scn11a*, *Mgat5b* were downregulated significantly in *Atoh1*$^{S193A/S193A}$ mice ($n = 5$; Fig. 6*C*). As would be predicted from the *in vitro* studies (Quan et al., 2016), we found that Atoh1-S193A bound promoter DNA of its target genes similarly to wild-type Atoh1, suggesting that the DNA-binding capacity of Atoh1-S193A is unimpaired *in vivo* (Fig. 6*E*). These results suggest that *Atoh1-S193A* is a hypomorphic allele that partially impairs Atoh1's ability to upregulate transcription of its target genes in the inner ear. This would likely lead to widespread transcriptional changes in the hair cell precursors, which we predict would ultimately affect the differentiation and survival of the hair cells.

Discussion

We have identified a phosphorylation site, S193, located in the evolutionarily conserved bHLH region of Atoh1. Mutation from the

serine to the nonphosphorylatable alanine, S193A, leads to a partial loss-of-function phenotype in mice. *Atoh1*$^{S193A/lacZ}$ mice performed poorly on the rotarod assay, had pontine nuclei progenitor migration defects and cerebellar foliation defects. *Atoh1*$^{S193A/lacZ}$ mice were profoundly deaf and had cochlear hair cell loss. In contrast, *Atoh1*$^{S193A/S193A}$ mice exhibited only moderate hearing deficits with cochlear hair cell loss at P21. These data suggest that there is a functional threshold for Atoh1 that varies with the cellular context.

It is interesting that *Atoh1* is downregulated shortly after birth in the inner ear with no transcripts detectable by P3 (Lanford et al., 2000), yet hair cell loss in the *Atoh1*$^{S193A/S193A}$ mice did not take place until P21. This suggests that the *Atoh1-S193A* mutation is not necessarily toxic to hair cells, but may cause less efficient activation of some transcripts, leading to loss of hair cell progenitors. The expression data of Atoh1 target genes in the inner ear support this theory: we found four examples of target genes that were downregulated significantly in *Atoh1*$^{S193A/lacZ}$ mice and two that were also downregulated significantly in *Atoh1*$^{S193A/S193A}$ mice. Both DNA-binding and protein interactions can affect a transcription factor's ability to upregulate its target genes properly. We have shown previously that Atoh1-S193A is able to bind DNA and heterodimerize with its obligate binding partners, the E proteins (Quan et al., 2016). However, given the transcriptional changes that we saw in the hair cells of *Atoh1*$^{S193A/lacZ}$ mice and the location of S193 in the protein interaction section of the bHLH domain, we hypothesize that Atoh1's ability to interact with other proteins that mediate coactivation of target genes may be impaired. It would be interesting to identify novel Atoh1-binding partners and then investigate whether Atoh1-S193A has decreased interactions with these proteins.

One surprising finding was the apparent hearing loss in the adult *Atoh1*$^{lacZ/+}$ mice. It has long been accepted that *Atoh1*$^{lacZ/+}$ mice are similar to wild-type mice (Ben-Arie et al., 1997; Fritzsch et al., 2005; Wang et al., 2005). However, the hearing loss at higher frequencies in these mice points to a possible haploinsufficiency phenotype. We did not see hair cell loss in the *Atoh1*$^{lacZ/+}$ mice before P21, indicating that the loss of hearing that we observed is due to either hair cell loss at a later time point or hair cell dysfunction. Atoh1 is highly expressed in the developing sensory epithelium; it is possible that lower

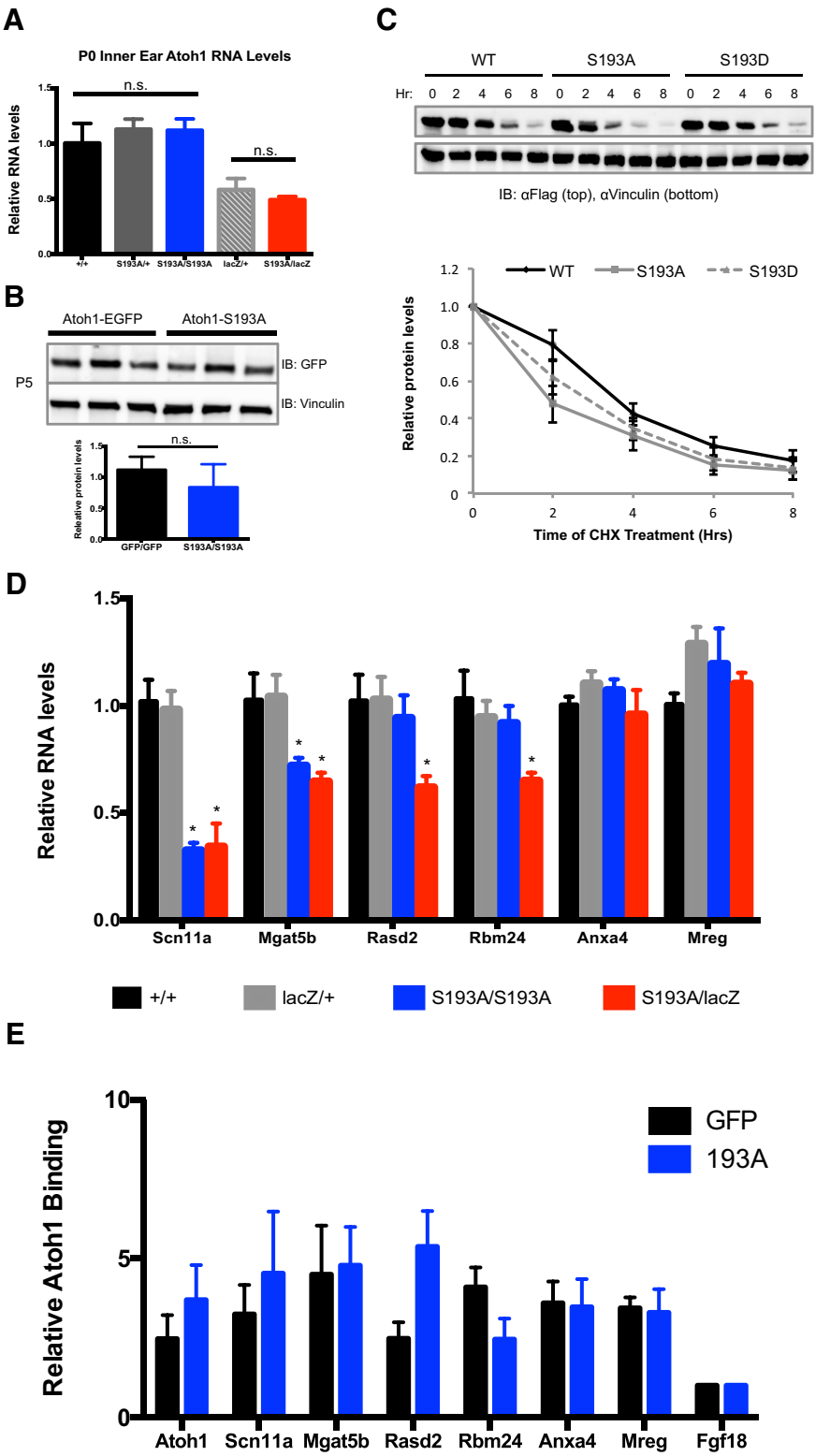

Figure 6. Some Atoh1 target genes in the inner ear have decreased expression in *Atoh1*$^{S193A/S193A}$ mice. ***A***, Quantitative RT-PCR analysis of Atoh1 RNA levels in P0 inner ears from *Atoh1*^{WT}, *Atoh1*$^{193A/+}$, *Atoh1*$^{193A/193A}$, *Atoh1*$^{LacZ/+}$, and *Atoh1*$^{193A/lacZ}$ mice ($n = 6$). Atoh1 transcript levels are representative of the number of alleles present. ***B***, Western blot analysis of Atoh1 protein levels in P5 cerebellum from *Atoh1*$^{GFP/GFP}$ and *Atoh1*$^{193A/193A}$ mice ($n = 3$). ***C***, Cycloheximide (CHX) pulse–chase assay. DAOY cells were transfected with wild-type, Atoh1–S193A, or Atoh1–S193D constructs. CHX (10 μg/ml) was added to cell media 24 h after transfection and cell lysates were collected at 0, 2, 4, 6, and 8 h after CHX addition. Atoh1 phospho-mutants have similar protein half-lives as wild-type Atoh1. Data are shown as mean ± SEM. ***D***, Quantitative RT-PCR analysis of selected Atoh1 target genes in the inner ear of P0 *Atoh1*^{WT}, *Atoh1*$^{193A/+}$, *Atoh1*$^{193A/193A}$, *Atoh1*$^{LacZ/+}$, and *Atoh1*$^{193A/lacZ}$ mice ($n = 5$). Data are shown as mean ± SEM. *$p < 0.05$, one-way ANOVA. ***E***, ChIP and quantitative PCR of selected Atoh1 target genes in the inner ear and *Atoh1* (positive control) and *Fgf18* (negative control) of P0 *Atoh1*$^{GFP/GFP}$ and *Atoh1*$^{193A/193A}$ mice ($n = 5$). Data are shown as mean ± SEM. n.s., Not significant.

levels of Atoh1 are sufficient for hair cell survival but cannot keep up with the transcriptional demand for hair cells to differentiate properly and become functional, eventually leading to their dysfunction or death.

It is intriguing that, although cochlear and vestibular hair cells come from the same pool of Atoh1-positive precursors, the hair cells in the vestibular system seem to be more resilient. Studies showed that deletion of Atoh1 from the cochlea before E15.5 leads to rapid cell death, whereas deletion of Atoh1 in the utricle only decreased expression of myosin VIIa, causing failure of stereocilia to form (Cai et al., 2013; Chonko et al., 2013). These early differences suggest that the transcriptional landscape differs between cochlear and utricle hair cells. Certainly, there are temporal differences between these two organs with regard to mechanical sensitivity: hair cells become mechanically sensitive between E16 and P0 in the utricle, but not until between P0 and P4 in the cochlea (Géléoc and Holt, 2003; Lelli et al., 2009).

It is also noteworthy that the inner hair cells of the cochlea seem to be the first and most affected in the *Atoh1-S193A* mice. This is unusual because most noise, blast, drug damage, and aging paradigms show that the outer hair cells are killed first (Govaerts et al., 1990; Bohne et al., 2000; Sha et al., 2008; Cho et al., 2013). One of the few examples of inner hair cells dying first is a study in which *Neurog1* was knocked into the *Atoh1* locus (Jahan et al., 2012). A milder phenotype was seen in a compound mutant of *Neurog1* knocked into the *Atoh1* locus together with a floxed *Atoh1* allele (Jahan et al., 2015). It is unclear why the inner hair cells are more sensitive to changes in Atoh1 levels or activity, but our findings have demonstrated a clear differential sensitivity among inner hair cells, outer hair cells, and utricle hair cells.

In addition to the inner ear hair cell defects, we discovered milder defects in pontine nucleus progenitor migration and missing foliation between lobules VI and VII of the cerebellum in the *Atoh1*$^{S193A/lacZ}$ mice. Although the anatomical defects in both the pontine nuclei and the cerebellum can contribute to the poor performance motor performance of the *Atoh1*$^{S193A/lacZ}$ mice, it is difficult to prove causality. However, associations between altered coordination and both pontine and cerebellar foliation defects have been described in humans and mice. Human patients with lesions in the basilar pons exhibit several motor coordination deficits (Schmahmann et al., 2004). In addition, mice with cerebellar foliation defects have motor coordination deficits (Chen et al., 2005, 2008, Rosin et al., 2015). One study in particular reported on motor coordination problems and the absence of lobule VI/VII foliation in *TR4*$^{-/-}$ mice that is strikingly similar to our cerebellar foliation defect (Chen et al., 2005).

We have shown previously that *Atoh1* is required for the birth and proliferation of rhombic lip progenitors; the absence of *Atoh1* results in the complete loss of mature neurons that derive from the rhombic lip, including both cerebellar granule and pontine nuclei neurons (Ben-Arie et al., 1997; Wang et al., 2005). In contrast, our present study suggests that not all neuronal progenitors from the rhombic lip are affected by the *Atoh1-S193A* mutation. The cerebellum is largely normal, suggesting that the CGNs are unaffected by the mutation. With the exception of the pontine nucleus, many other brainstem nuclei seem to be unaffected, suggesting that the pontine nuclei are the most affected lineage of the rhombic lip progenitors. The lack of foliation between lobules VI and VII could be due to less mossy fiber projection from the pontine nuclei. The cerebellum receives the majority of its mossy fiber input from the pontine nuclei and it has been shown that the pontine nuclei project heavily to lobules VI and VII in the cerebellum (Cicirata et al., 2005), implying a direct connection between the two phenotypes. This suggests that proper foliation of the mature cerebellum is dependent, not just on the cells populating the cerebellum, but also on proper projections from distant neurons.

Other phosphorylation sites of Atoh1 have been described previously (Tsuchiya et al., 2007; Forget et al., 2014; Cheng et al., 2016). Serines 52 and 56 were shown to affect Atoh1 stability. These findings, however, were not reproduced (Tsuchiya et al., 2007; Cheng et al., 2016). Serines 328, 339, and 334 have also been implicated in altering Atoh1 stability, specifically through interactions with E3 ubiquitin ligase Huwe1 (Forget et al., 2014; Cheng et al., 2016). These sites are located in the serine-rich C-terminal domain found only in vertebrate homologs of Atoh1 (Mulvaney and Dabdoub, 2012). S193, however, is located in the highly conserved bHLH domain and is thus found, not only in humans and other vertebrate species, but also in flies. In addition, S193 does not seem to affect Atoh1 protein stability, but rather, mimicking phosphorylation (S193D) at this residue abolishes Atoh1's ability to bind DNA, rendering the phospho-mutant protein functionally null (Quan et al., 2016).

A recent study characterized mice carrying a methionine to isoleucine mutation in the bHLH region (M200I; *Atoh1*$^{trhl/trhl}$; Sheykholeslami et al., 2013). Similar to our *Atoh1-S193A* mice, *Atoh1*$^{trhl/trhl}$ mice present with hearing loss and loss of cochlear hair cells. In addition, *Atoh1*$^{trhl/trhl}$ mice have a trembling gait and smaller cerebella with a lack of foliation in all lobules, indicating that this M200I point mutation results in a stronger hypomorphic phenotype than our *Atoh1-S193A* mice. It was not tested whether the M200I point mutation alters DNA binding, dimerization with E proteins, or transcriptional activity of Atoh1, but it is likely that at least one of these functions is affected given its location in the bHLH region.

In sum, we have created and characterized an Atoh1 knock-in mouse bearing a mutation in the most evolutionarily conserved serine of the bHLH. Our mouse model will be a useful tool with which to study Atoh1 function in specific cell populations while circumventing the perinatal death phenotype that is seen in the *Atoh1*-null mouse. The effect of *Atoh1-S193A* on other *Atoh1*-dependent cell populations is currently unknown, but would be worthy of investigation. Most importantly, this work may contribute to a better understanding of the genetics behind human deafness, which affects one in every 500 newborns and 278 million individuals worldwide (Shearer and Smith, 2012). We propose that *Atoh1* haploinsufficiency and *Atoh1* point mutations may cause human deafness, particularly later-onset hearing loss, in the absence of other symptoms.

References

Ben-Arie N, Bellen HJ, Armstrong DL, McCall AE, Gordadze PR, Guo Q, Matzuk MM, Zoghbi HY (1997) Math1 is essential for genesis of cerebellar granule neurons. Nature 390:169–172. CrossRef Medline

Ben-Arie N, Hassan BA, Bermingham NA, Malicki DM, Armstrong D, Matzuk M, Bellen HJ, Zoghbi HY (2000) Functional conservation of atonal and Math1 in the CNS and PNS. Development 127:1039–1048. Medline

Bermingham NA, Hassan BA, Price SD, Vollrath MA, Ben-Arie N, Eatock RA, Bellen HJ, Lysakowski A, Zoghbi HY (1999) Math1: an essential gene for the generation of inner ear hair cells. Science 284:1837–1841. CrossRef Medline

Bermingham NA, Hassan BA, Wang VY, Fernandez M, Banfi S, Bellen HJ, Fritzsch B, Zoghbi HY (2001) Proprioceptor pathway development is dependent on Math1. Neuron 30:411–422. CrossRef Medline

Bohne BA, Harding GW (2000) Degeneration in the cochlea after noise damage: primary versus secondary events. Am J Otol 21:505–509. Medline

Cai T, Seymour ML, Zhang H, Pereira FA, Groves AK (2013) Conditional

deletion of Atoh1 reveals distinct critical periods for survival and function of hair cells in the organ of Corti. J Neurosci 33:10110–10122. CrossRef Medline

Cai T, Groves AK (2015a) The role of Atonal factors in mechanosensory cell specification and function. Mol Neurobiol 52:1315–1329. CrossRef Medline

Cai T, Jen HI, Kang H, Klisch TJ, Zoghbi HY, Groves AK (2015b) Characterization of the transcriptome of nascent hair cells and identification of direct targets of the Atoh1 transcription factor. J Neurosci 35:5870–5883. CrossRef Medline

Chao HT, Chen H, Samaco RC, Xue M, Chahrour M, Yoo J, Neul JL, Gong S, Lu HC, Heintz N, Ekker M, Rubenstein JL, Noebels JL, Rosenmund C, Zoghbi HY (2010) Dysfunction in GABA signalling mediates autism-like stereotypies and Rett syndrome phenotypes. Nature 468:263–269. CrossRef Medline

Chen P, Johnson JE, Zoghbi HY, Segil N (2002) The role of Math1 in inner ear development: Uncoupling the establishment of the sensory primordium from hair cell fate determination. Development 129:2495–2505. Medline

Chen YT, Collins LL, Uno H, Chang C (2005) Deficits in motor coordination with aberrant cerebellar development in mice lacking testicular orphan nuclear receptor 4. Mol Cell Biol 25:2722–2732. CrossRef Medline

Chen YT, Collins LL, Chang SS, Chang C (2008) The roles of testicular orphan nuclear receptor 4 (TR4) in cerebellar development. Cerebellum 7:9–17. CrossRef Medline

Cheng YF, Tong M, Edge AS (2016) Destabilization of Atoh1 by E3 ubiquitin ligase Huwe1 and casein kinase 1 is essential for normal sensory hair cell development. J Biol Chem 291:21096–21109. CrossRef Medline

Chien CT, Hsiao CD, Jan LY, Jan YN (1996) Neuronal type information encoded in the basic-helix-loop-helix domain of proneural genes. Proc Natl Acad Sci U S A 93:13239–13244. CrossRef Medline

Cho SI, Gao SS, Xia A, Wang R, Salles FT, Raphael PD, Abaya H, Wachtel J, Baek J, Jacobs D, Rasband MN, Oghalai JS (2013) Mechanisms of hearing loss after blast injury to the ear. PLoS One 8:e67618. CrossRef Medline

Chonko KT, Jahan I, Stone J, Wright MC, Fujiyama T, Hoshino M, Fritzsch B, Maricich SM (2013) Atoh1 directs hair cell differentiation and survival in the late embryonic mouse inner ear. Dev Biol 381:401–410. CrossRef Medline

Cicirata F, Zappala A, Serapide MF, Parenti R, Panto MR, Paz C (2005) Different pontine projections to the two sides of the cerebellum. Brain Res Brain Res Rev 49:280–294. CrossRef Medline

Flora A, Garcia JJ, Thaller C, Zoghbi HY (2007) The E-protein Tcf4 interacts with Math1 to regulate differentiation of a specific subset of neuronal progenitors. Proc Natl Acad Sci U S A 104:15382–15387. CrossRef Medline

Forget A, Bihannic L, Cigna SM, Lefevre C, Remke M, Barnat M, Dodier S, Shirvani H, Mercier A, Mensah A, Garcia M, Humbert S, Taylor MD, Lasorella A, Ayrault O (2014) Shh signaling protects Atoh1 from degradation mediated by the E3 ubiquitin ligase Huwe1 in neural precursors. Dev Cell 29:649–661. CrossRef Medline

Fritzsch B, Matei VA, Nichols DH, Bermingham N, Jones K, Beisel KW, Wang VY (2005) Atoh1 null mice show directed afferent fiber growth to undifferentiated ear sensory epithelia followed by incomplete fiber retention. Dev Dyn 233:570–583. CrossRef Medline

Géléoc GS, Holt JR (2003) Developmental acquisition of sensory transduction in hair cells of the mouse inner ear. Nat Neurosci 6:1019–1020. CrossRef Medline

Gnedeva K, Hudspeth AJ (2015) SoxC transcription factors are essential for the development of the inner ear. Proc Natl Acad Sci U S A 112:14066–14071. CrossRef Medline

Govaerts PJ, Claes J, van de Heyning PH, Jorens PG, Marquet J, De Broe ME (1990) Aminoglycoside-induced ototoxicity. Toxicol Lett 52:227–251. CrossRef Medline

Groves AK, Zhang KD, Fekete DM (2013) The genetics of hair cell development and regeneration. Annu reverse Neurosci 36:361–381. CrossRef Medline

Haque K, Pandey AK, Zheng HW, Riazuddin S, Sha SH, Puligilla C (2016) MEKK4 signaling regulates sensory cell development and function in the mouse inner ear. J Neurosci 36:1347–1361. CrossRef Medline

Huang WH, Tupal S, Huang TW, Ward CS, Neul JL, Klisch TJ, Gray PA, Zoghbi HY (2012) Atoh1 governs the migration of postmitotic neurons that shape respiratory effectiveness at birth and chemoresponsiveness in adulthood. Neuron 75:799–809. CrossRef Medline

Jahan I, Pan N, Kersigo J, Calisto LE, Morris KA, Kopecky B, Duncan JS, Beisel KW, Fritzsch B (2012) Expression of Neurog1 instead of Atoh1 can partially rescue organ of Corti cell survival. PLoS One 7:e30853. CrossRef Medline

Jahan I, Pan N, Kersigo J, Fritzsch B (2015) Neurog1 can partially substitute for Atoh1 function in hair cell differentiation and maintenance during organ of Corti development. Development 142:2810–2821. CrossRef Medline

Klisch TJ, Xi Y, Flora A, Wang L, Li W, Zoghbi HY (2011) In vivo Atoh1 targetome reveals how a proneural transcription factor regulates cerebellar development. Proc Natl Acad Sci U S A 108:3288–3293. CrossRef Medline

Lanford PJ, Shailam R, Norton CR, Gridley T, Kelley MW (2000) Expression of Math1 and HES5 in the cochleae of wildtype and Jag2 mutant mice. J Assoc Res Otolaryngol 1:161–171. CrossRef Medline

Lelli A, Asai Y, Forge A, Holt JR, Géléoc GS (2009) Tonotopic gradient in the developmental acquisition of sensory transduction in outer hair cells of the mouse cochlea. J Neurophysiol 101:2961–2973. CrossRef Medline

Maricich SM, Wellnitz SA, Nelson AM, Lesniak DR, Gerling GJ, Lumpkin EA, Zoghbi HY (2009) Merkel cells are essential for light-touch responses. Science 324:1580–1582. CrossRef Medline

Matsuura K, Kabuto H, Makino H, Ogawa N (1997) Pole test is a useful method for evaluating the mouse movement disorder caused by striatal dopamine depletion. J Neurosci Methods 73:45–48. CrossRef Medline

Mulvaney J, Dabdoub A (2012) Atoh1, an essential transcription factor in neurogenesis and intestinal and inner ear development: function, regulation, and context dependency. J Assoc Res Otolaryngol 13:281–293. CrossRef Medline

Pan N, Jahan I, Kersigo J, Kopecky B, Santi P, Johnson S, Schmitz H, Fritzsch B (2011) Conditional deletion of Atoh1 using Pax2-Cre results in viable mice without differentiated cochlear hair cells that have lost most of the organ of Corti. Hear Res 275:66–80. CrossRef Medline

Quan XJ, Yuan L, Tiberi L, Claeys A, De Geest N, Yan J, van der Kant R, Xie WR, Klisch TJ, Shymkowitz J, Rousseau F, Bollen M, Beullens M, Zoghbi HY, Vanderhaeghen P, Hassan BA (2016) Post-translational control of the temporal dynamics of transcription factor activity regulates neurogenesis. Cell 164:460–475. CrossRef Medline

Rose MF, Ahmad KA, Thaller C, Zoghbi HY (2009) Excitatory neurons of the proprioceptive, interoceptive, and arousal hindbrain networks share a developmental requirement for Math1. Proc Natl Acad Sci U S A 106:22462–22467. CrossRef Medline

Rose MF, Ren J, Ahmad KA, Chao HT, Klisch TJ, Flora A, Greer JJ, Zoghbi HY (2009) Math1 is essential for the development of hindbrain neurons critical for perinatal breathing. Neuron 64:341–354. CrossRef Medline

Rosin JM, McAllister BB, Dyck RH, Percival CJ, Kurrasch DM, Cobb J (2015) Mice lacking the transcription factor SHOX2 display impaired cerebellar development and deficits in motor coordination. Dev Biol 399:54–67. CrossRef Medline

Schmahmann JD, Ko R, MacMore J (2004) The human basis pontis: motor syndromes and topographic organization. Brain 127: 1269–91. CrossRef Medline

Sha SH, Kanicki A, Dootz G, Talaska AE, Halsey K, Dolan D, Altschuler R, Schacht J (2008) Age-related auditory pathology in the CBA/J mouse. Hear Res 243:87–94. CrossRef Medline

Shearer AE, Smith RJ (2012) Genetics: advances in genetic testing for deafness. Curr Opin Pediatr 24:679–686. CrossRef Medline

Sheykholeslami K, Thimmappa V, Nava C, Bai X, Yu H, Zheng T, Zhang Z, Li SL, Liu S, Zheng QY (2013) A new mutation of the Atoh1 gene in mice with normal life span allows analysis of inner ear and cerebellar phenotype in aging. PLoS One 8:e79791. CrossRef Medline

Tsuchiya K, Nakamura T, Okamoto R, Kanai T, Watanabe M (2007) Reciprocal targeting of Hath1 and beta-catenin by Wnt glycogen synthase kinase 3beta in human colon cancer. Gastroenterology 132:208–220. CrossRef Medline

Untergasser A, Nijveen H, Rao X, Bisseling T, Geurts R, Leunissen JA (2007) Primer3Plus, an enhanced web interface to Primer3. Nucleic Acids Res 35:W71–4. CrossRef Medline

Wang VY, Hassan BA, Bellen HJ, Zoghbi HY (2002) *Drosophila* atonal fully rescues the phenotype of Math1 null mice: new functions evolve in new cellular contexts. Curr Biol 12:1611–1616. CrossRef Medline

Wang VY, Rose MF, Zoghbi HY (2005) Math1 expression redefines the rhombic lip derivatives and reveals novel lineages within the brainstem and cerebellum. Neuron 48:31–43. CrossRef Medline

Wang X, Spandidos A, Wang H, Seed B (2012) PrimerBank: a PCR primer database for quantitative gene expression analysis, 2012 update. Nucleic Acids Res 40:D1144–9. CrossRef Medline

Yang Q, Bermingham NA, Finegold MJ, Zoghbi HY (2001) Requirement of Math1 for secretory cell lineage commitment in the mouse intestine. Science 294:2155–2158. CrossRef Medline